Applied Catalysis B: Environmental 225 (2018) 30–39

Contents lists available at ScienceDirect

Applied Catalysis B: Environmental

journal homepage: www.elsevier.com/locate/apcatb

Bone char-derived metal-free N- and S-co-doped nanoporous carbon and its efficient electrocatalytic activity for hydrazine oxidation

André L. Cazetta[a], Tao Zhang[b], Taís L. Silva[c], Vitor C. Almeida[a,**], Tewodros Asefa[b,d,*]

[a] Laboratory of Environmental and Agrochemistry, Department of Chemistry, The State University of Maringá, 5790 Colombo Avenue, Maringá 87020-900, Paraná, Brazil
[b] Department of Chemical and Biochemical Engineering, Rutgers, The State University of New Jersey, 98 Brett Road, Piscataway, NJ 08854, USA
[c] Federal University of Technology – Paraná, 635 Marcílio Dias Street, Apucarana, Paraná, Brazil
[d] Department of Chemistry and Chemical Biology, Rutgers, The State University of New Jersey, 610 Taylor Road, Piscataway, New Jersey 08854, USA

ARTICLE INFO

Keywords:
Metal-free electrocatalyst
Carbon electrocatalyst
Hydrazine oxidation
Template synthesis
Nitrogen and sulfur co-doped carbon

ABSTRACT

Bone char (BC) was successfully used, for the first time, both as a self-template/a pore-former and a precursor of heteroatoms (N and S atoms) during carbonization of sucrose, allowing for the synthesis of nanoporous N- and S-co-doped carbon (NSC) material possessing high surface area and excellent electrocatalytic activity. BC's ability to help with the formation of nanopores in the carbon material was indirectly confirmed by making a control material, denoted as pyrolyzed sucrose or PS, under the same condition but without including BC in the reaction media. N_2 gas porosimetry showed that NSC had a very large BET surface area (1108 $m^2 g^{-1}$), which is about 60% higher than that of PS (443 $m^2 g^{-1}$). Comparison of the SEM images of the two materials also indicated some differences in their textural and morphological features. XPS analysis showed that NSC had a higher content of S (2.29%) than PS (0.21%) and that the S atoms were distributed mostly in the form of thiophenic moieties (32.3% for the PS and 59.2% for the NSC). Although some of the S groups were originated from sulfuric acid, which was used for the dehydration of sucrose during the synthesis of the materials, this result indicated that BC was the major source of the S dopant atoms in NSC as well as the major reason for the formation of thiophenic groups in this material. Furthermore, while PS's structure did not have N dopants, NSC's lattice had about 1.39% of N dopant atoms that existed in the form of pyridinic, pyrrolic and graphitic groups and that were also originated from BC. X-ray diffraction and Raman spectroscopy revealed that NSC's lattice had a higher density of defects than PS. Owing to its high surface area and optimal density of heteroatom dopant groups and defect sites, NSC exhibited excellent electrocatalytic activity toward the hydrazine oxidation reaction (HzOR), or the lowest overpotential ever reported for this reaction, along with a high current density. Besides making it among the most efficient electrocatalysts for HzOR, its electrocatalytic performance can make this metal-free material a good alternative to the conventional metal-based electrocatalysts that are commonly used in HzOR-based fuel cells.

1. Introduction

The increase in energy demand worldwide has long prompted the scientific and engineering community to find alternative energy sources that can reduce our reliance on fossil fuels [1]. As part of this effort, substantial attention has focused on direct liquid fuel cells (DLFCs), which can convert chemical energy sources such as ethanol, methanol, dihydrogen (H_2), low molecular weight hydrocarbons, and others into electrical energy [2,3]. However, for these promising energy systems to efficiently generate electrical energy directly from chemical fuels, they require advanced, effective catalysts, which can efficiently promote the half-reactions involved at the electrodes of the fuel cells [4].

Most catalytic active materials used at the anode and cathode in many conventional fuel cells contain less earth-abundant noble metals such as Pt and Ir; consequently, fuel cells are currently expensive and hard to scale up for large-scale commercial applications [2]. This also means, less costly and sustainable fuel cells catalysts should be developed in order for fuel cells to become viable for large-scale applications and make major differences in our renewable energy landscapes [2]. Non-noble metal-based alternative catalysts that have been widely investigated in recent years to replace conventional fuel cell catalysts include non-precious metals and metal alloys. Such materials have been reported to effectively catalyze reactions such as the oxygen reduction reaction (ORR) [5,6], the ethanol oxidation reaction (EOR) [7], the

* Corresponding author at: Department of Chemical and Biochemical Engineering, Rutgers, The State University of New Jersey, 98 Brett Road, Piscataway, New Jersey 08854, USA.
** Corresponding author.
E-mail addresses: vcalmeida@uem.br (V.C. Almeida), tasefa@rci.rutgers.edu (T. Asefa).

https://doi.org/10.1016/j.apcatb.2017.11.050
Received 20 June 2017; Received in revised form 2 October 2017; Accepted 17 November 2017
Available online 21 November 2017
0926-3373/

hydrogen evolution reaction (HER) [8], the hydrazine oxidation reaction (HzOR) [9,10], etc. There have also been several reports in the literature, where various metals and metallic alloys in supported forms on other materials, mainly carbons and metal oxides, could serve as catalysts for these types of reactions [11–13]. In fact, many commercially used catalysts for various reactions are available in supported forms, except that they comprise noble metals (*e.g.*, Pt/C) [7,14]. Many of them are synthesized by anchoring or "heterogenizing" catalytically active metallic species on solid-state support materials. However, the use of metals and metallic alloys as catalysts even in supported forms still presents some challenges especially in electrocatalysis, due to the possible dissolution, corrosion, poisoning, sintering and/or agglomeration of the metals in the catalysts [15]. This is often what leads to the reduction in activity or the complete failure of these catalysts over time.

In addition to various bare noble metals and metal alloys and their supported variants, heteroatom-doped carbon-based materials (*e.g.*, N-doped carbons) containing metals have been considered as promising electrocatalysts for many reactions [2]. Studies have indicated that the catalytic activities of these materials, for the most part, stem from their chemical dopant groups and the perturbation of the electron configurations in their lattice as a result of the heteroatom dopant atoms. Additionally, in the presence of some supported metals, the dopant groups of many such materials form highly catalytically active sites [16]. However, these catalysts too have some drawbacks such as high cost of synthesis, low selectivity to desired products and poor stability, besides the sintering, leaching and corrosion problems mentioned above [17].

Hence, considerable efforts have recently been directed toward the development of metal-free carbon materials for application as catalysts in various catalytic processes [2]. To make carbon materials effective electrocatalysts, generally their carbon lattices should be doped with the right types of heteroatom dopants or dopant moieties. In particular, doping carbon structures with elements such as N and S atoms makes these materials highly electrocatalytically active. This is because N and S dopant atoms easily modulate the conjugated sp^2-sp^2 linkages, π-orbital electron delocalization, and electron distribution in the structures of these materials. These, in turn, generate positively and negatively charged groups on the materials that are often effective in adsorbing reactants or intermediates, desorbing the products, and promoting the overall conversions of the reactants into desired products [17,18]. The dopants also improve the steps associated with bond breakages in the reactants or bond formations in the products during electrocatalysis [17]. So, materials that can help these processes and provide the right balance of adsorption and desorption processes with less energy barriers are highly desirable in electrocatalysis.

To synthesize such types of heteroatom-doped carbon-based materials, researchers have tried various methods as well as several types of precursors. In many cases, graphite and graphene oxide were used as starting materials [20–23], while in many others, more sustainable carbon sources, such as cellulosic paper [18], rice grains [1], yeast cells [12], cotton [3,24], sucrose [25], softwood kraft pulp-derived cellulose nanofibrils [26], etc. were applied. The use of sustainable carbon sources for making these materials is obviously more appealing in order to be able to ultimately scale up the synthesis and the production of catalysts in large scales for fuel cells. However, it is additionally necessary to replace or eliminate the many toxic and non-environmentally friendly chemicals, such as ammonium hydroxide, pyrrole, and *N,N*-dimethylformamide, which are often used for the synthesis of heteroatom-doped carbon materials.

In this report, bone char (BC) is successfully shown, for the first time, to serve as a low-cost precursor of N and S dopant atoms as well as a self-template for the synthesis of high surface area, electrocatalytically active, nanoporous N- and S-co-doped carbon (NSC). For the synthesis of NSC, sucrose was used as the main source of carbon and subjected to carbonization in the presence of BC. The resulting NSC material was found to efficiently electrocatalyze the hydrazine oxidation reaction (HzOR). The benefits of BC in resulting this catalytically active carbon material was indirectly determined by making a control material from sucrose without including BC in the precursor. This material, which was denoted as pyrolyzed sucrose (PS), did not catalyze HzOR as much as NSC did. On the other hand, thanks to BC, NSC showed more catalytically beneficial textural, chemical and morphological features (high surface area and more heteroatom dopants) compared with PS. HzOR, the reaction that the reported materials were tested to catalyze here, is a highly important electrochemical reaction for fuel cells. This is because, if operated against ORR, HzOR generates only environmental-friendly compounds (N_2 and H_2O) while giving off a high theoretical cell voltage (+1.61 V) and producing a high-energy density (5400 W h L^{-1}). In other words, direct hydrazine fuel cells can generate more energy per unit mole than many other DLFCs and typical H_2-powered fuel cells, while producing environmentally friendly by-products [3,9,27].

2. Materials and methods

2.1. Reagents and chemicals

Commercial-grade sucrose (União brand, refined sugar) was purchased from a local supplier of União Company in Brazil. Hydrochloric acid (37%), sulfuric acid (98%), 2-propanol, Nafion (5% in a solution of lower aliphatic alcohols and water, in which 15–20% is water), hydrazine monohydrate (98%) and phosphate buffer saline (10X PBS, pH 6.8) were purchased from Sigma-Aldrich, USA. All the chemicals and reagents were used as received without further purification.

2.2. Synthesis of N- and S-co-doped carbon (NSC)

BC, the material that was employed as a hard-template in the synthesis of the NSC reported herein, was obtained using an optimized synthetic procedure described in our previous report [28]. Then, 1.00 g of BC was mixed with 1.25 g of sucrose, 5.00 g of distilled water, and 0.14 g of sulfuric acid in a polytetrafluoroethylene (PTFE)-coated reactor. The mixture/reactor was kept in oven at 100 °C for 6 h, and then heated to 160 °C and kept at this temperature for 6 h. A dark-colored product was obtained, which was ground to powder using a mortar and pestle. After putting the resulting powder product back inside the reactor, more sucrose (0.80 g), sulfuric acid (0.09 g) and distilled water (5.00 g) were mixed with it. The mixture was then heated under the same conditions as described above. The final product was ground to powder and then put in a crucible and pyrolyzed in a muffle furnace (EDG-S equipment EDG3P 7000) as follows. First, it was heated from room temperature to 450 °C at a heating rate of 5 °C min^{-1} and kept at this temperature for 2 h under a flow of N_2 atmosphere that was let to flow at a rate of 100 cm^3 min^{-1}. After this time, the N_2 atmosphere was replaced by a flow of CO_2 that was also let to flow at the same rate of 100 cm^3 min^{-1}. The furnace temperature was increased from 450 °C to 750 °C at a heating rate of 5 °C min^{-1} and then kept at this temperature for 3 h. After this time, the furnace was programmed to cool down to *ca.* 150 °C in 4 h under a flow of N_2 at a rate of 100 cm^3 min^{-1}. The resulting pyrolyzed material was treated with an aqueous solution of HCl (50 mL, 1.0 mol L^{-1}) in an autoclave at 110 °C for 6 h in order to remove the BC through dissolution. This procedure was performed three times, by replacing the HCl solution with a fresh one. The solid product was washed several times with hot, distilled water (the temperature of which was *ca.* 60 °C) until the pH of the supernatant reached *ca.* 6.5. For each purification step (using acidic solution, followed by distilled water), the supernatant was removed by vacuum filtration with a membrane (Millipore, 0.45 μm). The equilibrium that describes the dissolution of BC in acidic media can be given as follows, Eq. (1) [29].

$$Ca_{10}(OH)_2(PO_4)_6(s) + 8H^+(aq) \rightleftharpoons 10Ca^{2+}(aq) + 6HPO_4^{-2}(aq) + 2H_2O \quad (1)$$

For comparative studies, another carbon material was synthesized by using a higher amount of BC (2.00 g) under otherwise the same synthetic conditions and procedure as the one used to make the original NSC. The resulting material was labeled as NSC2. To evaluate the effectiveness of BC as a hard-template for the synthesis of the nanoporous carbon materials, a control material labeled as PS (pyrolyzed sucrose) was obtained without using BC as a hard template, also under otherwise the same synthetic procedure and condition as described above.

2.3. Characterization of materials

The pore properties of PS, NSC and NSC2 were measured with N_2 porosimetry at 77 K using a surface area and pore size analyzer, Nova 1200e (QuantaChrome). The BET specific surface area (S_{BET}) values of the materials were calculated from the linear fit of the data in the N_2 adsorption/desorption isotherms in the relative pressure range (p/p°) of 0.05–0.20 using the Brunauer-Emmett-Teller (BET) equation. The total pore volume (V_t) was obtained from the maximum amount of N_2 adsorbed in each material at a relative pressure of 0.99. The micropore volume (V_μ) of each material was calculated using the *α(s)-plot* method, and the mesopore volume (V_m) of each material was obtained using the BJH method. The average pore size (A_{PS}) of the material was calculated using the equation $4\ V_t/S_{BET}$, and the pore size distribution of each material was obtained using a method developed based on the non-local density functional theory (NLDFT) [30].

The morphological features of PS and NSC were investigated with scanning electron microscopy (SEM) using a Quanta™ FEG 250 microscope (FEI Company) without metallizing the samples. The functional groups present on the materials were investigated with Fourier transform infrared spectroscopy (FTIR) using a Shimadzu IRTracer-100 FTIR spectrometer. The spectra were obtained with an acquisition rate of 32 scan min^{-1} and a resolution of 4 cm^{-1} in a range of 400–4000 cm^{-1}. Samples for the measurements were prepared as pellets with KBr. The materials were also analyzed with X-ray photoelectron spectroscopy (XPS) using a Thermo Scientific K-Alpha X-ray photoelectron Spectrometer. Some of the XPS peaks were deconvoluted for further analysis. X-ray diffraction (XRD) patterns of the materials were obtained using a Shimadzu XRD-7000 diffractometer operating with Cu Kα (λ = 1.5406 Å) as the X-ray beam source. The XRD patterns of the materials were acquired in a 2θ range of 10–80° with a step size of 0.02° and an acquisition time of 5 s. The micro Raman spectra of the materials were recorded using a Brüker dispersive Raman microscope operating at a wavelength (λ) of 532 nm. The spectra were acquired with a scan rate of 10 scans min^{-1} in a range of 500–2500 cm^{-1}.

2.4. Electrochemical and electrocatalytic studies

The electrochemical and electrocatalytic properties of the materials toward HzOR were measured using a PAR Versasat3 instrument (Princeton Applied Research). Cyclic voltammetry was performed in a potential range of 0.1 to 1.3 V *vs.* RHE at a scan rate of 10 mV s^{-1} using 15 mL hydrazine solution with concentrations ranging from 0 to 50 mM in a phosphate buffer saline (PBS 1X, pH 7.4). The experiments were carried out in an electrochemical cell possessing a three-electrode configuration, composed of a calomel saturated electrode (SCE) as a reference electrode, a platinum wire as a counter electrode and a glassy carbon electrode containing the NSC or PS as a working electrode. To obtain the working electrode, 2 μL of a homogeneous suspension of catalyst (NSC, NSC2 or PS) with a concentration of 0.10 g L^{-1} in 2-propanol was prepared and casted on a glassy carbon electrode, then coated with Nafion (2 μL, 5% in 2-propanol), and finally let to dry in air for 5 min. Chronoamperometric analysis was performed at a potential of 0.58 V *vs.* RHE using 50 mM hydrazine solution. The equations used to calculate the number of electrons involved in HzOR are described in the Supplementary Information (SI) section.

3. Results and discussion

3.1. Synthesis and characterization of PS and NSC

The synthesis of N- and S-co-doped carbon, which was denoted as NSC, was carried out using BC as a hard-template as well as a source of the heteroatom dopants. As discussed below, owing to its textural and structural features as well as compositions, BC served both these functions well enough and resulted in carbon materials with the right structural features and heteroatom-dopants to be very good electrocatalysts for HzOR. The BC we employed for this purpose was synthesized using an optimized synthetic procedure previously reported by our research group [28]. The material possessed exclusively mesoporous structure with an average pore size of 10.3 nm and a BET surface area of 128 $m^2\ g^{-1}$. Furthermore, BC contained proteins, which are composed of type I collagen or amino acids such as glycine, proline, hydroxyproline and hydroxylysine (which contain amine groups) as well as cysteine and methionine (which contain amine and thiol/thioether groups) [31]. Thus, besides serving as a hard template, the BC was able to deliver N and S heteroatom dopants into the carbon material forming from sucrose through carbonization. The ability of BC to help with the formation of heteroatom-doped carbon (*i.e.*, NSC) materials was evaluated by making a control material, denoted as PS, from sucrose without including BC, and then comparing the properties of the two materials with each other (see below).

The textural properties of the two materials were investigated first by N_2 porosimetry. The results, which are displayed in Fig. 1a and b, indicated that PS and NSC had different N_2 adsorption/desorption isotherms. The isotherm obtained for PS (Fig. 1a) could be classified as

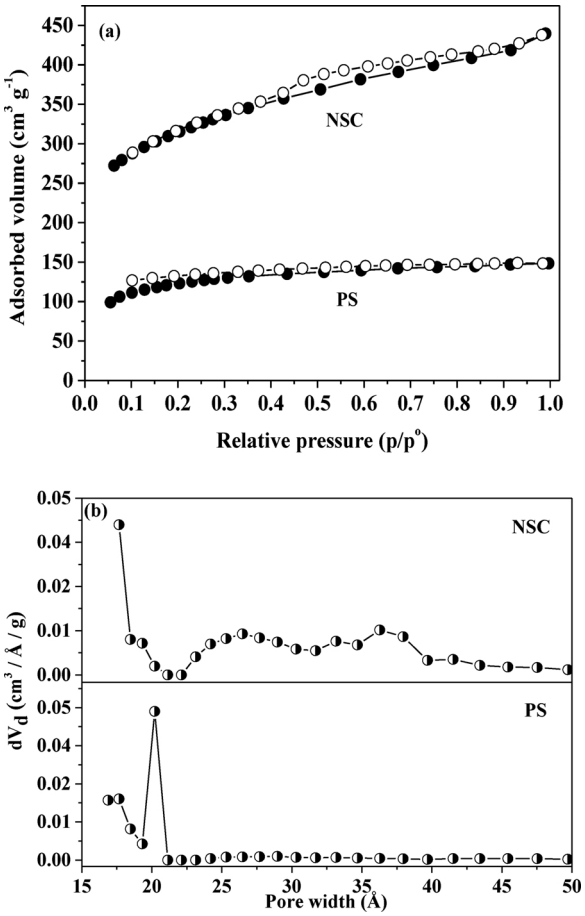

Fig. 1. N_2 adsorption/desorption isotherms of (a) N and S-co-doped carbon (NSC) and pyrolyzed sucrose (PS or the control material) and (b) their respective pore size distribution obtained by the NLDFT method.

Table 1
Textural properties of control material (PS) and N- and S-co-doped carbon (NSC).

	PS	NSC
BET surface area value ($m^2\ g^{-1}$)	443	1108
Total pore volume ($cm^3\ g^{-1}$)	0.23	0.68
Micropore volume ($cm^3\ g^{-1}$)	0.08	0.23
Mesopore volume ($cm^3\ g^{-1}$)	0.03	0.21
Average pore size (nm)	2.1	2.5

Type-I, which is characteristic of microporous materials [32]. On the other hand, the isotherm obtained for NSC could be classified as *Type-IV*, with *H4*-hysteresis loop and a capillary condensation step at high relative pressure ($P/P°$) (between 0.45–0.80), which is characteristic of mesoporous structures [18,20,33]. The textural properties of both materials calculated from their corresponding isotherms are compiled in Table 1.

According to the results displayed in Table 1, using BC as a hard-template clearly helped with the formation of a carbon material with very large surface area (1108 $m^2\ g^{-1}$), which was *ca.* 60% higher than that of PS, the BET surface area of which was only 443 $m^2\ g^{-1}$. Moreover, the total pore volume (V_t) of NSC was concomitantly larger (0.68 $cm^3\ g^{-1}$), which was *ca.* 66% more than that of PS. The average pore sizes of NSC and PS were found to be 2.5 and 2.1 nm, respectively. The pore size distributions of both materials were analyzed and compared with one another (Fig. 1b). The results showed that the pores in PS were distributed in a narrow range (between 1.8 and *ca.* 2.1 nm) with the maximum centered at *ca.* 2.0 nm whereas the pores in NSC were distributed in a wide range, starting at *ca.* 1.9 nm and extending all the way to *ca.* 4.0 nm.

Based on the FTIR spectra, the types of functional groups present in PS and NSC were determined. The FTIR spectra of PS and NSC (Fig. 2) showed three bands centered at *ca.* 3300, 1600 and 1100 cm^{-1}, which could be assigned to O—H stretching vibration of carboxylic groups, C=C stretching of non-oxidized aromatic domains and stretching in —CH—OH moieties, respectively [20,22]. Additionally, in the FTIR spectrum of NSC, a band centered at *ca.* 1750 cm^{-1}, which is characteristic of the stretching vibration of C—OOH groups, and a band at *ca.* 1380 cm^{-1}, which can be assigned to the stretching vibration of C—N groups, were identified. The band observed at *ca.* 1220 cm^{-1} was assigned to the stretching vibration of C = S groups [34,35], and the band at *ca.* 1060 cm^{-1} in the spectrum of NSC was attributed to —CH—OH bond stretching [22]. Based on the results, it was clear that NSC had N and S dopant groups in it.

To obtain more detailed information about the functional groups on

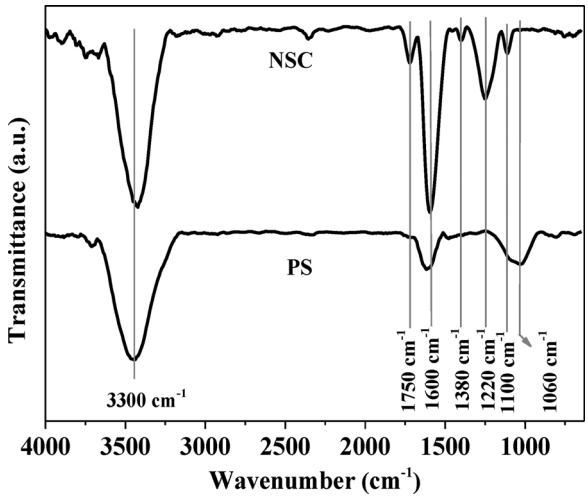

Fig. 2. FTIR spectra of PS and NSC.

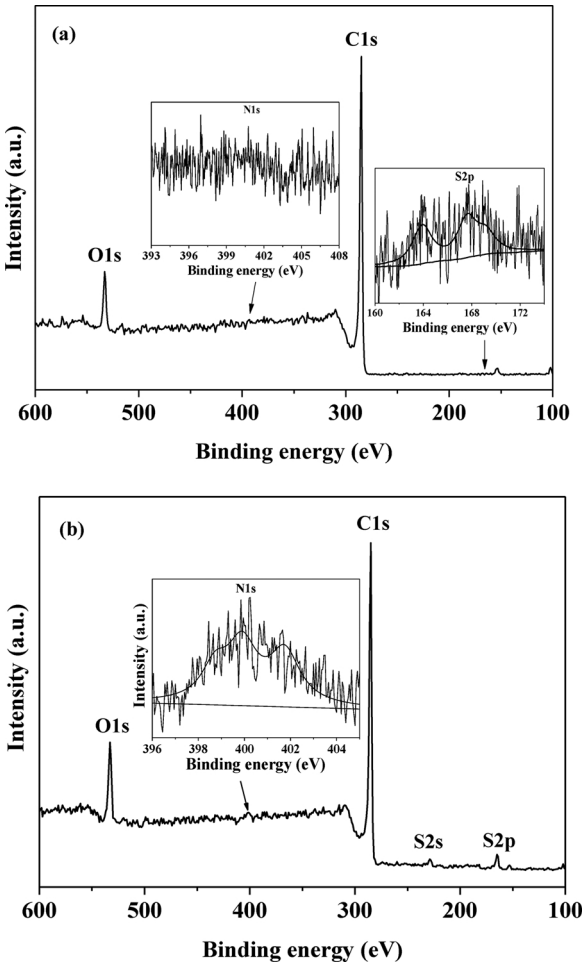

Fig. 3. XPS survey spectra of PS and NSC.

the surfaces of the materials, XPS survey spectra were obtained (Fig. 3a and b), and the peaks were then analyzed. The XPS spectrum of PS (Fig. 3a) showed three distinct peaks centered at *ca.* 164, 285 and 532 eV associated with S 2p, C 1s and O 1s [36,37], suggesting the presence of these three elements in this material. Analysis of the N 1s region in the XPS spectrum indicated the absence of N in this material, as expected (see the inset in Fig. 3a). Based on the spectra, the relative compositions of S, C and O on the surfaces of PS were found to be 0.2%, 91.2% and 8.6%, respectively. The small amount of S observed in PS (see inset in Fig. 3a) was most likely originated from sulfuric acid, which was used for the dehydration of sucrose during the synthesis of the carbon materials. The ability of sulfuric acid to incorporate S atoms into related materials was previously reported by others. For example, Huang and Fu [38] reported that the use of concentrated sulfuric acid as a dehydrating agent for natural polymers and sugars led to the formation of sulfopolycyclic aromatic species during the synthesis of carbon materials from these precursors. Moreover, pyrolysis of various S-containing precursors at higher temperature was reported to result in higher amount of S dopant atoms in carbon materials [39].

On the other hand, the XPS survey spectrum of NSC (Fig. 3b) showed the characteristic peaks associated with S at *ca.* 164 eV (S 2p) and 229 eV (S 2s), C at *ca.* 285 eV, and O at *ca.* 532 eV. The spectrum further showed the characteristic peak of N 1s, centered at *ca.* 400 eV, indicating the presence of N [37] in this material. The spectrum revealed that the relative compositions of S, C, N and O in this material were 2.29%, 86.10%, 1.39% and 10.20%, respectively. These results clearly demonstrated the effectiveness of BC as precursor to provide N and S heteroatom dopants into a carbon material, yielding the N- and S-co-doped carbon material. This is besides BC's proven ability to serve as

a hard template and make the material nanoporous, as discussed earlier.

The high-resolution XPS spectra of S 2p, C 1s and N 1s peaks for both NSC and PS were deconvoluted, and the results were compiled (see Table S1 and Fig. S1a–e). The high-resolution C1s peak of PS (Fig. S1a) was deconvoluted into four peaks centered at *ca.* 284.7, 286.1, 287.3 and 289.8 eV corresponding to C═C groups (93.25%), carbon atoms in C-S and C−O species (3.28%), carbon atoms in C═O groups (1.95%), and carbon atoms in O−C═O groups (1.52%), respectively. For NSC, the high-resolution C 1s peak (Fig. S1b) also showed four distinct peaks centered at *ca.* 284.7, 286.4, 287.4 and 290.0 eV, which could be attributed to C═C moieties (82.55%), carbon atoms in C−S and C−O groups (12.35%), carbon atoms in C−N and C═O groups (3.27%), and carbon atoms in O−C═O (1.85%), respectively [26,36,40,41]. It is worth pointing out here that the high intensity of the peaks associated with C−S and C−N groups in the spectrum of NSC once again had to do with BC. In other words, BC was responsible for the formation of a carbon material doped with N and S dopant atoms.

Similarly, the high-resolution spectra of S 2p peak of PS and NSC were deconvoluted (Fig. S1c and d). Based on the similarities and differences of their spectra, it was possible to identify four distinct peaks. For the PS material (Fig. S1c), peaks at *ca.* 163.4 and 165.1 eV, which are attributable to C−S−C groups (with S $2p_{3/2}$ = 32.3% and S $2p_{1/2}$ = 9.7% that are characteristic of spin-orbit coupling of S-thiophenic groups) were seen. Additionally, peaks at *ca.* 168.1 and 172.1 eV, associated with the S atoms in C-SO_3 (40.0%) and C−SO_4 (18.0%) groups, respectively, were observed. The deconvolution of the S 2p high-resolution peak in the spectrum of NSC (Fig. S1d) showed peaks centered at *ca.* 164.1 and 165.2 eV, which could be assigned to C−S−C groups (with S $2p_{3/2}$ = 59.2% and S $2p_{1/2}$ = 30.8%), and peaks at *ca.* 167.4 and 168.7 eV, which could be assigned to C-SO_2 (7.25%) and C-SO_3 (2.71%) moieties, respectively [9,29,42,43]. From these results, it could be said that using BC along with the carbon precursor (*i.e.*, sucrose) enabled a higher amount of thiophenic groups to form in the carbon lattice. In addition, it could be said that including BC in the precursor resulted in significantly less amount of oxidized S species in the material. There is clearly also a large difference in the amount of S between the two materials: NSC has 2.29% of S but PS has only 0.21% of S. So, although the sulfuric acid used as a dehydrating agent during the synthesis of the materials definitely contributed to some of the S dopants in NSC (since 0.21% of S was seen also in PS), most of the S dopants in NSC (*ca.* 91%) were originated from BC. Meanwhile, when the high-resolution spectrum of N 1s peak of NSC was deconvoluted (Fig. S1e), it showed three peaks centered at *ca.* 398.7, 399.9 and 401.8 eV associated with pyridinic N (20.43%), pyrrolic N (42.17%) and graphitic N groups (37.40%), respectively [3,35,44].

The X-ray diffraction (XRD) patterns of NSC and PS (Fig. 4a) showed two peaks at 2θ of *ca.* 23.2° and 43.4°, which are characteristic of the C(001) and C(100/101) reflection planes of non-crystalline and crystalline/graphitic (sp^2-hybridized) carbon, respectively [3,21]. The intensity of the XRD peak centered at *ca.* 43.4° was lower in the case of NSC, the material made using BC in the precursor. This could be due to the fact that BC introduced more heteroatoms into the carbon lattice, as discussed above, and thereby created more defect sites in the carbon material.

The effect of BC had on the crystallinity of the carbon material could be appreciated further by comparing the Raman spectrum of PS with that of NSC (Fig. 4b). The spectra of both materials presented two bands at *ca.* 1337 cm^{-1} and 1594 cm^{-1} corresponding to the characteristic D and G bands (disordered and sp^2-ordered C structures), respectively [22,12]. The ratio of the intensity of the two peaks, I_D/I_G, for PS and NSC were found to be 0.92 and 0.94, respectively, indicating that NSC had slightly more defect sites in its structure than PS. This result was well in line with those obtained by XRD, FTIR and XPS analyses, which also indicated that NSC had more dopants and its structural features were different from PS.

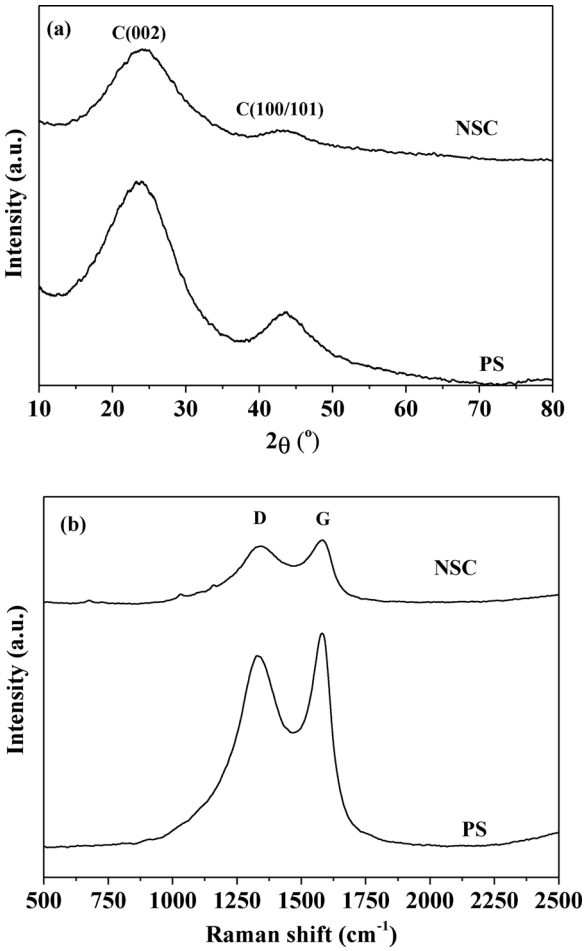

Fig. 4. (a) XRD patterns and (b) Raman spectra of PS and NSC.

The morphological features of PS and NSC were compared with each other by obtaining SEM images for both materials (Fig. 5). The SEM image of PS (Fig. 5a and b) showed that the material had smooth surface features or not much surface roughness. On the other hand, the SEM images of NSC (Fig. 5c and d) showed more heterogeneous and rougher surfaces, which also seemed to be the reason behind the observed inter-particle pores in it. These results further indicated the ability of BC to cause some morphological and textural modifications in the carbon material, in line with the results discussed earlier.

3.2. Electrocatalytic performance of NSC

The electrocatalytic performance of heteroatom-doped carbon-derived materials is known to be highly dependent on three major materials' properties, namely: *(i)* the presence/absence of vacant/defect sites in the materials, *(ii)* the presence/absence of specific dopant groups in the materials and *(iii)* the surface area/pore structures/conductivity of the materials [1,3,35]. As mentioned above, the introduction of heteroatom dopant atoms, such as N atoms, into the lattice of carbon materials can alter the materials' band gaps. It can also lead to a decrease in the distance between the conduction and the valence bands as well as in the electron work function of the materials, enabling higher degrees of electron mobility at their solid/liquid interfaces. This is why the presence of dopant species in the carbon lattice generally renders enhanced electrocatalytic activities to the materials toward various reactions.

Additionally, heteroatom doping of carbon materials can enhance the electron transfer in the materials; this is because of the ability of the dopant atoms to accept or donate lone pair electrons and give rise to a

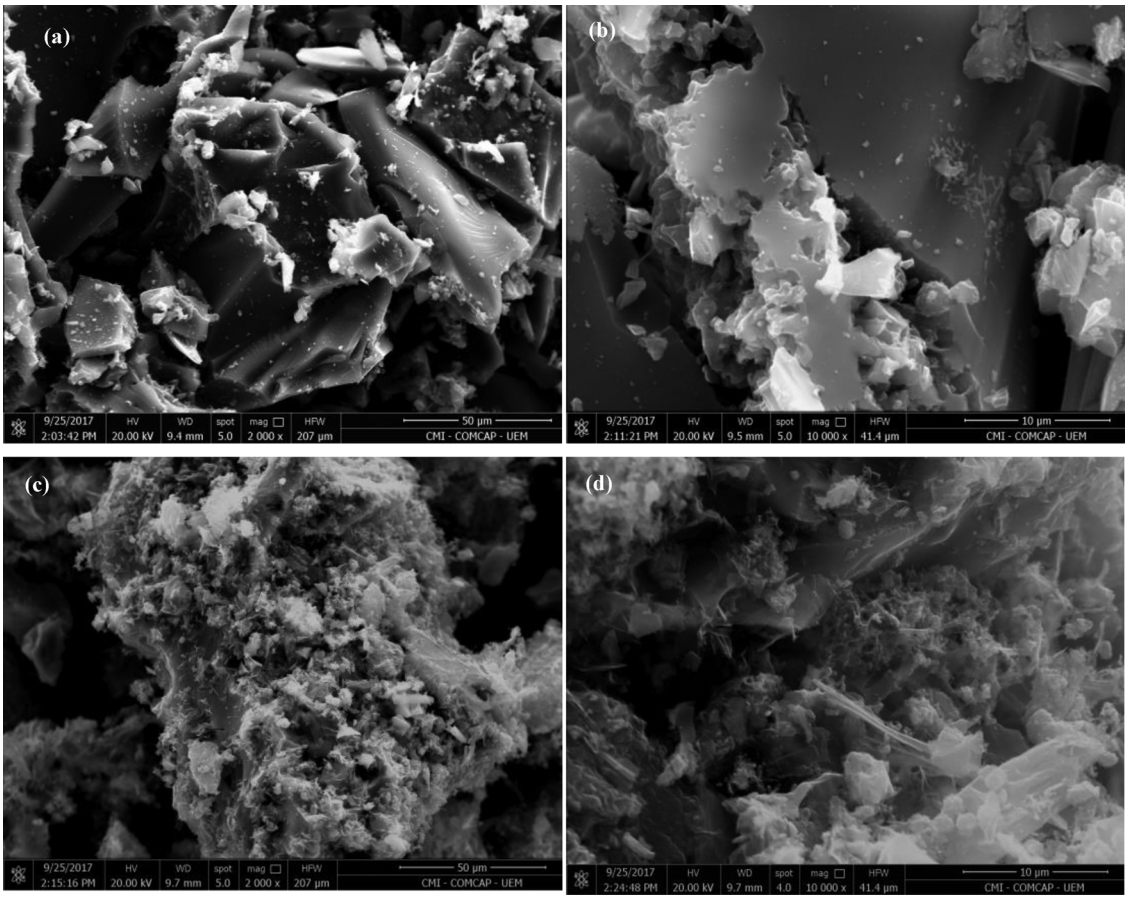

Fig. 5. SEM images of PS (a and b) and NSC (c and d) materials.

region in the material with apparent difference in charge density with respect to the carbon atoms around them [19,16,45]. This can, in turn, improve the electron mobility through the surfaces of the catalyst, promoting catalytic conversions. However, the ability of the heteroatom dopants to do these varies from one type of heteroatom to another. For example, despite its relatively lower electronegativity compared with a N atom, a S dopant atom in carbon materials could create a higher degree of structural defect because of its larger atomic size (110 pm) compared with that of a N atom (65 pm); as a result, the former tends to form regions in the carbon materials that could adsorb reacting substances (*e.g.* hydrazine during HzOR) better. Additionally, the empty orbital in *3p* level of S could accommodate the lone pair of electrons of reacting substances during the electrocatalytic processes, and then assist them with their transformations into the products better [2,19]. Finally, it is worth noting why the surface area and pore structures of the heteroatom-doped carbon materials can affect their electrocatalytic performances. Like in many traditional catalysts, the surface area and pore structures of carbon-based catalysts can dictate the accessibility of the catalytic sites in the materials to reactants and intermediates as well as the conductivity of the materials [16]. However, although a higher surface area might improve mass diffusion in the materials, it might not guarantee that the heteroatom-doped carbon would have good electrocatalytic activity because higher surface might also lead to lower conductivity in the materials.

So, for a carbon material to be highly electrocatalytically active, it must have well-structured porosity and specific dopant atoms/species in its lattice. Hence, NSC can be expected to be a good electrocatalyst since it meets these criteria. On the other hand, the control material PS may not be as suitable, because it does not have high contents of N and S dopant atoms and its surface area is significantly lower. The electrocatalytic properties of the two materials for HzOR were experimentally evaluated with cyclic voltammetry in the presence of 50 mM hydrazine solution in PBS (pH 7.4). The result, displayed in Fig. 6a, clearly showed that PS had a much lower electrocatalytic activity than NSC for HzOR. The onset potential of the reaction over PS was found to be 0.81 V *vs.* RHE, while that over NSC was found to be 0.38 V *vs.* RHE (which corresponds to 2.13-fold more negative onset potential than that of PS). This means, a much higher potential (overpotential) should be applied to realize the same degree of hydrazine oxidation over PS compared with what is needed to start the HzOR over NSC. Additionally, the peak potential for NSC for a hydrazine concentration of 50 mM was seen at *ca.* 0.65 V *vs.* RHE with an associated current density of 2.88 mA cm^{-2} whereas the corresponding value for PS was 0.99 V *vs.* RHE with a current density of 1.93 mA cm^{-2}. Due NSC's superior electrocatalytic performance, as demonstrated above, the remaining studies were carried out only for NSC.

The cyclic voltammograms (CVs) of HzOR over NSC at different concentrations of hydrazine solution (ranging from 0 to 100 mM) were then acquired and analyzed (Fig. 6b). The current density in the CVs was found to be proportional to the concentration of hydrazine in the concentration range we conducted the study here (see Fig. S2 in Supplementary Information section). Additionally, the shape of the CVs showed only an oxidation peak or an irreversible process, confirming the existence of hydrazine oxidation. The catalytic property of NSC was compared with different catalytically active materials reported for HzOR in the literature (see Table 2). Although precise comparison was not possible, because different experimental conditions were employed by different research groups to evaluate the catalytic efficiency of the materials reported in their works, it was still apparent from Table 2 that NSC had a better electrocatalytic activity for HzOR than many electrocatalysts reported recently in the literature. Furthermore, the onset potential (0.38 V *vs.* RHE) obtained for NSC was comparable with some

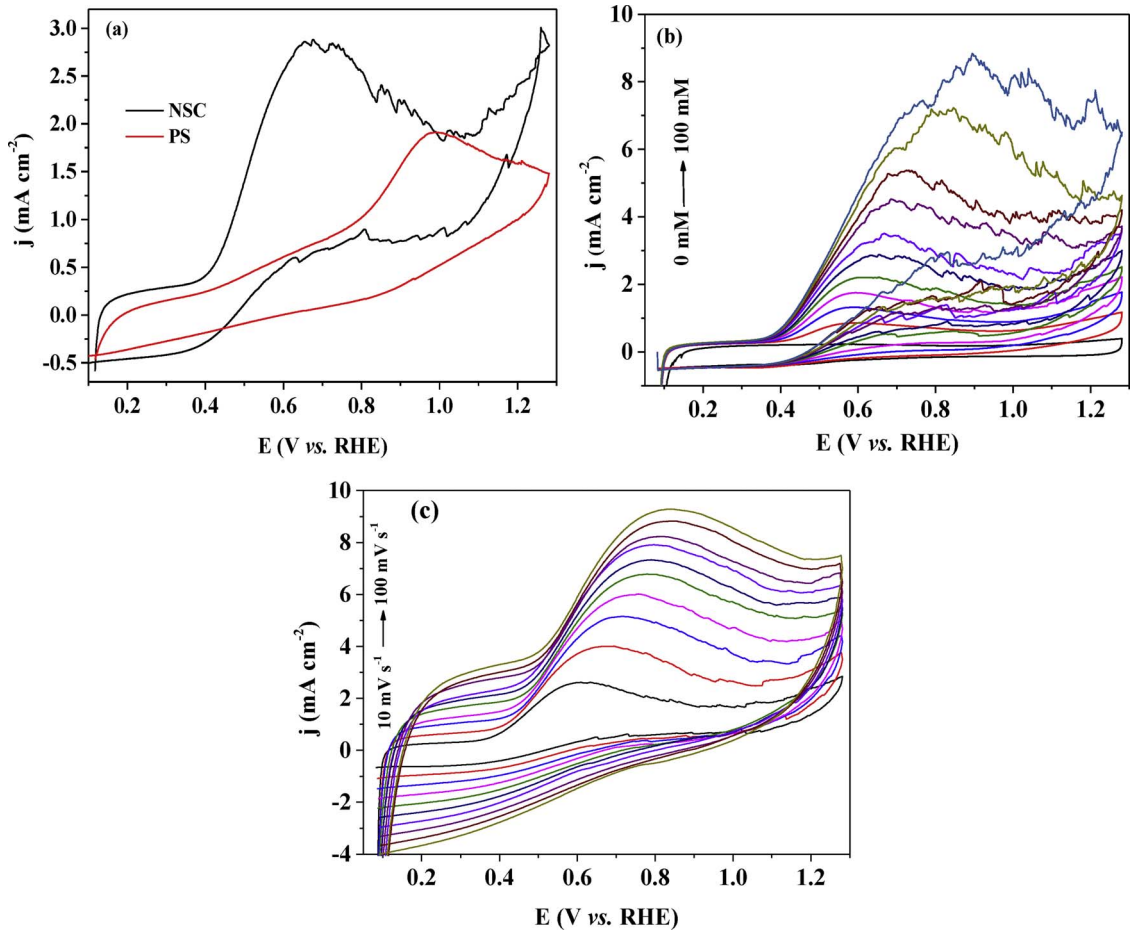

Fig. 6. (a) Cyclic voltammograms of hydrazine oxidation reaction (HzOR) over PS and NSC materials acquired using 50 mM hydrazine solution in PBS (pH 7.4) at scan rate of 10 mV s^{-1}, (b) cyclic voltammograms of HzOR obtained using different concentrations of hydrazine at a scan rate of 10 mV s^{-1} in a 0.1 M PBS solution (pH 7.4) over NSC electrocatalyst and (c) cyclic voltammograms of HzOR obtained with 50 mM hydrazine in 0.1 M PBS solution at pH 7.4 at different scan rates over NSC electrocatalyst.

of the best performing catalysts reported for HzOR found in the literature. For comparative discussion, the potentials that were not expressed as "*vs.* RHE" in the authors' works were converted here to "vs. SCE" using the equation: $E_{RHE} = E_{read} + E^{\circ}_{reference} + 0.059$ pH. For example, Yu et al. [23] synthesized N-doped holey graphene, which electrocatalyzed HzOR with an onset potential of 0.53 V *vs.* RHE. The electrocatalytic activity of NSC for HzOR was also comparable with that of polypyrrole-derived metal-free, N- and O-co-doped mesoporous carbon electrocatalyst reported by us before and which showed the best catalytic performance for HzOR so far, with an onset potential of 0.32 V *vs.* RHE [15]. NSC's electrocatalytic performance for HzOR was also better than the catalytic activity of NiCuP amorphous alloy reported by Wang and coworkers [46],which catalyzed the reaction at an onset potential of 0.45 V *vs.* RHE.

The cyclic voltammograms of HzOR over NSC at different scan rates were then obtained (Fig. 6c), and the kinetics of the reaction was determined (see Figs. S3 and S4 and Supporting Information for more details). The diffusion coefficient (D) was estimated by the Cottrell equation using the linear correlation obtained between the current density (I/A) and the inverse square root of the time ($t^{-1/2}$) (Fig. S4a).

Table 2
Comparison of the electrocatalytic properties of the different carbon materials reported here for hydrazine oxidation reaction (HzOR) with those of other related carbon materials reported in the literature for the same reaction.

Material	Medium	Scan rate (mV s^{-1})	[N_2H_4] (mM)	Peak potential (V *vs.* RHE)	Onset potential (V *vs.* RHE)	Reference
N-S-doped carbon	PBS	10	50	0.65[a]	0.39[a]	[3]
Flower-shaped CuO	KOH	50	100	–	0.79	[9]
G/NiCuCo alloy	NaOH	100	400	1.67[a]	–	[10]
N-doped carbon	PBS	10	50	0.74[a]	0.38[a]	[18]
N-doped carbon	PBS	50	5	1.02[a]	0.76[a,b]	[35]
Cu_3P/CF	KOH	5	500	–	0.03[b]	[47]
CoS_2/TiM	KOH	5	100	–	0.01[b]	[48]
Ni_2P/NF	KOH	5	500	–	−0.05[b]	[49]
CoP/TiM	KOH	5	100	–	−0.05[b]	[50]
NiS_2/TiM	KOH	5	500	–	0.05[b]	[51]
FeP NA/NF	KOH	5	500	–	0.02[b]	[52]
NSC	**PBS**	**10**	**50**	**0.60**	**0.38**	**Current work**

[a] Obtained by converting the reported potential to "*vs.* RHE" from the equation: $E_{RHE} = E_{read} + E^{\circ}_{reference} + 0.059$ pH.
[b] Estimated the CV curves obtained with LSV.

The total number of electron (n) involved in the reaction was calculated and found to be close to 4, implying the occurrence of nearly complete oxidation of hydrazine over NSC. The value of n was not exactly 4, because not 100% of hydrazine is often converted to N_2 and H_2O during the reaction, as some are likely to end up at intermediate species and then remain adsorbed onto the carbon material during the reaction [18]. Additionally, the use of peak-fitted equations on the experimental data obtained from chronoamperometry and cyclic voltammetry could lead to slight deviations in the values of n with respect to what is expected theoretically. The reactions that describe the hydrazine oxidation are shown in equations below (Eqs. (2)–(4)), and they involve a net loss of four electrons transforming hydrazine first to diazene and then to N_2, with each involving two electrons [15,47].

$$N_2H_4 + 2OH^- \rightarrow N_2H_2 + 2H_2O + 2e^- \quad (2)$$

$$N_2H_2 + 2OH^- \rightarrow N_2 + 2H_2O + 2e^- \quad (3)$$

$$\text{Net:} \quad N_2H_4 + 4OH^- \rightarrow N_2 + 4H_2O + 4e^- \quad (4)$$

To check the effect of the degree of N and S doping on the materials' electrocatalytic properties, the structure and electrocatalytic property of NSC2, the carbon material prepared by using a relatively higher amount of BC under otherwise the same synthetic conditions and procedure as those used to make the original NSC, were studied. The relative surface composition of NSC2 was determined based on the XPS survey spectrum of the material (Fig. S5), and the amounts of C, N, O and S on the surfaces of NSC2 were found to be 70.69, 4.27, 17.77 and 7.27%, respectively (*cf.*, the corresponding values of NSC are 86.10, 1.39, 10.20 and 2.29%, respectively). The results indicated that increasing the relative amount of bone char for the synthesis of the carbon material (NSC2) led to a substantial increase in the amount of S and N dopants in the materials, by around 3-fold for S and by about 3-fold for N, compared with those of NSC. Additionally, the textural properties of NSC2 were characterized and the results were compared with those of NSC. The results, which are summarized in Table S2, suggested that the increase of the amount of bone char for the synthesis of the carbon material (NSC2) led to a decrease in the BET surface area (730 $m^2\,g^{-1}$, compared with that of NSC 1108 $m^2\,g^{-1}$) but an increase in the average pore size in the material ($\approx$2.4-fold higher than the average pore size of NSC).

Next, the electrocatalytic activities of NSC2 for HzOR was tested also using 50 mM hydrazine solution in PBS with cyclic voltammometry at a scan rate of 10 mV s^{-1}, and the result is compared with that of NSC (see Fig. S6). Based on the results, NSC2 could be seen to have lower electrocatalytic activity for HzOR than NSC, since the former gave a higher overpotential and a lower current density in the reaction than NSC did. So, overall, the results suggested that the increase in the contents of heteroatoms in these carbon materials did not necessarily render them higher electrocatalytic activity for HzOR, as NSC2, which has higher amounts of N and S dopant atoms, showed lower catalytic activity than NSC did. As discussed earlier, the increase in the amount of bone char for the synthesis of the material led to an increase in the average pore size, which in turn can gave rise to more defects in the carbon structure and thereby lower electron mobility (conductivity) through the material. Therefore, NSC2's lower electrocatalytic performance toward HzOR could be the result of its higher pore diameter, and thereby larger defect sites and lower conductivity of its carbon lattice. On the other hand, the higher surface area and possible lower defect sites in NSC may have been responsible for its better electrocatalytic activity toward HzOR compared with NSC2.

Alkaline media are strongly recommended in many types of electrocatalytic reactions especially those containing non-noble metal-based catalysts, because alkaline media result in faster reaction kinetics and reasonable power output and also because many non-noble metal-based catalysts are stable at higher pH [48–53]. Performing electrocatalysis in electrolytes with pH near neutral values is equally, or sometimes more, attractive, because neutral media are environmentally benign and safer to use. Furthermore, the performances of some electrocatalysts in some reactions, including HzOR, can be good in neutral media. For example, Galabi and Mirzazadeh [54] showed that the peak current during electrocatalytic HzOR increased when the pH was increased from lower pH to 6.5 and then remained the same up to pH 7.5, but then decreased when the pH was further increased. The authors suggested that the decrease in electrocatalytic activity of the material at higher pH was most likely due to the decrease in the surface coverage of the electrode in more alkaline solution. It is worth adding here that electrocatalytic HzOR have been successfully carried out in electrolytes with near neutral pH over metal-free heteroatom-doped carbon materials before [55,56]. So, in order to check if this would also be the case for the catalysts reported here and to determine the effect of electrolyte in the catalytic performance of NSC, the CV of 50 mM hydrazine solution in KOH (0.1 mol L^{-1}) using Hg/HgO (E° = 0.098 V *vs.* NHE) electrode as a reference electrode was recorded. The result is then compared with the CV recorded for 50 mM hydrazine solution in PBS (0.1 mol L^{-1}) obtained using SCE (E° = 0.244 V *vs.* NHE) as a reference electrode (Fig. S7).

As expected, the results showed that the electrolyte plays an important role in the electrocatalytic performance of NSC material toward HzOR. In alkaline media, the onset potential was found to be 0.47 V *vs.* RHE and the peak potential was found to be centered at *ca.* 0.79 V *vs.* RHE with an associated current density of 6.06 mA cm^{-2}. However, in the electrolyte with pH near neutral value (PBS, pH 7.4), the values were found to be 0.38 V *vs.* RHE, 0.60 V *vs.* RHE and 2.88 mA cm^{-2}, respectively. Clearly, the onset potential was shifted toward positive values (by 90 mV) when an alkaline media was used as electrolyte. On the other hand, the maximum current density increased $\approx$2.10-fold in alkaline media (which could be associated with an increase in the Faradaic efficiency). The shift of the onset and peak potentials to more positive values in alkaline solutions compared with those obtained in near-neutral electrolyte (PBS) means an increase in overpotential required for HzOR in alkaline media. Thus, to conduct HzOR electrocatalysis with a good balance between onset potential value and maximum current density, PBS solution appears to be a reasonable electrolyte for the materials reported here.

Finally, the stability of NSC as electrocatalysts was evaluated by chronoamperometry (Fig. 7a). The results showed that the residual current after running the HzOR over NSC for 5400 s did not change much, indicating the relative stability of the material as a catalyst during the HzOR. Besides the chronoamperometric test, the stability of the NSC catalyst toward HzOR was investigated by cycling the reaction many times (Fig. 7b). After 800 cycles, the retention peak current density was barely changed, indicating once again the high stability of NSC as electrocatalyst for HzOR. The results overall demonstrated that BC could be used as a precursor of heteroatoms as well as a template, allowing the synthesis of efficient metal-free carbon electrocatalyst—a potential noble metal alternative electrocatalyst for HzOR in direct hydrazine fuel cells.

4. Conclusion

In this work, the use of bone char (BC) both as a precursor of N and S dopant atoms and as a hard-template for making N- and S-co-doped nanoporous carbon (NSC) with high surface area, large density of heteroatom dopants and very good electrocatalytic activity for HzOR has been demonstrated. In the synthesis, sucrose has been used the main source of carbon in the materials. This is the first time that BC was successfully used as a hard-template as well as heteroatom doping agent producing a metal-free carbon electrocatalyst. The textural and morphological characterization of NSC and its corresponding control material (PS, obtained without using BC) indicated the ability of BC to serve as a pore former, resulting in a nanoporous carbon material with high surface area (NSC), *ca.* 60% higher surface area than the control

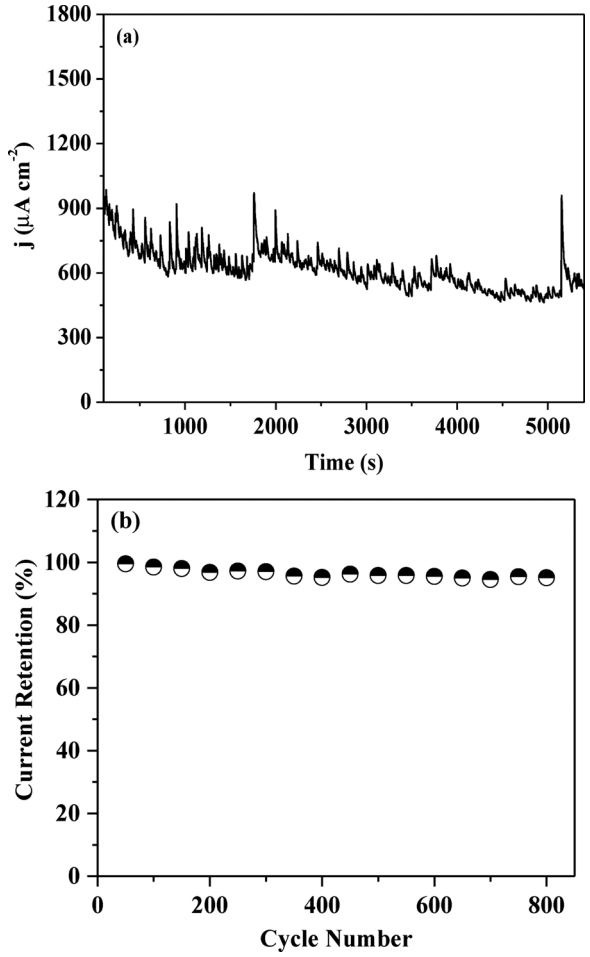

Fig. 7. (a) Chronoamperometric curve and (b) stability test results of HzOR over NSC obtained at a potential of 0.58 V *vs.* RHE for 50 mM of hydrazine in a 0.1 M PBS solution at pH 7.4. (Note that the spikes in the graph are caused by bubbles of N_2 formed during HzOR. When these bubbles form, they limit the accessible surfaces on the electrocatalyst, limiting the amount of current that is generated by the electrocatalyst, causing the dips. This effect is quite common in HzOR).

material made without BC (PS). Additionally, the effectiveness of BC to serve as a precursor of N and S dopant atoms has been determined by chemical analyses of both materials. The presence of both N and S heteroatom dopants in NSC's lattice has been confirmed to do mainly with BC. Their high surface area combined with their pyridinic N, pyrrolic N, graphitic S and thiophenic S groups have made NSC to exhibit high electrocatalytic activity toward HzOR with low overpotential while giving high current density. NSC's electrocatalytic performances also make it to be among the best metal-free electrocatalysts reported for HzOR to date. Thus, the material has a great potential to serve as sustainable metal-free electrocatalyst for HzOR in direct hydrazine fuel cells.

Acknowledgments

ALC and VCA acknowledge the financial support provided by the Conselho Nacional de Desenvolvimento Científico e Tecnológico (CNPq-Brazil) for their doctoral and postdoctoral fellowships, respectively, and the research work (Grant number: 484306/2013-8). TA gratefully acknowledges the financial support of the U.S. National Science Foundation (Grant No.: DMR-1508611) for allowing his group to pursue the work reported in this article.

Appendix A. Supplementary data

Supplementary data associated with this article can be found, in the online version, at http://dx.doi.org/10.1016/j.apcatb.2017.11.050.

References

[1] K. Koh, Y. Meng, X. Huang, X. Zou, M. Chhowalla, T. Asefa, N- and O-doped mesoporous carbons derived from rice grains: efficient metal-free electrocatalysts for hydrazine oxidation, Chem. Commun. 52 (2016) 13588–13591.
[2] T. Asefa, Metal-free and noble metal-free heteroatom-doped nanostructured carbons as prospective sustainable electrocatalysts, Acc. Chem. Res. 49 (2016) 1873–1883.
[3] E.H. Fragal, V.H. Fragal, X. Huang, A.C. Martins, T.S.P. Cellet, G.M. Pereira, E. Mikmeková, A.F. Rubira, R. Silva, T. Asefa, From ionic liquid-modified cellulose nanowhiskers to highly active metal-free nanostructured carbon catalysts for the hydrazine oxidation reaction, J. Mater. Chem. A 5 (2017) 1066–1077.
[4] L. Wei, H.E. Karahan, S. Zhai, Y. Yuan, Q. Qian, K. Goh, A.K. Ng, Y. Chen, Microbe-derived carbon materials for electrical energy storage and conversion, J. Energy Chem. 25 (2016) 191–198.
[5] Y. Yang, C. Dai, Y. Shen, A. Fisher, D. Cheng, Design of binary and ternary platinum shelled electrocatalysts with inexpensive metals for the oxygen reduction reaction, Int. J. Hydrogen Energy 41 (2016) 13014–13023.
[6] C.A. Cortés-Escobedo, R.D.G. González-Huerta, A.M. Bolarín-Miró, F. Sánchez De Jesús, Q. Zhu, S.E. Canton, K. Suarez-Alcantara, M. Tufiño-Velazquez, Mechanically activated Pt-Ni and Pt-Co alloys as electrocatalysts in the oxygen reduction reaction, Int. J. Hydrogen Energy 39 (2014) 16722–16730.
[7] M. Sánchez, A.R. Pierna, A. Lorenzo, J.J. Del Val, Effect of cocatalyst and composition on catalytic performance of amorphous alloys for ethanol electrooxidation and PEMFCs, Int. J. Hydrogen Energy 41 (2016) 19749–19755.
[8] C.I. Müller, K. Sellschopp, M. Tegel, T. Rauscher, B. Kieback, L. Röntzsch, The activity of nanocrystalline Fe-based alloys as electrode materials for the hydrogen evolution reaction, J. Power Sources 304 (2016) 196–206.
[9] Y. Ma, H. Wang, J. Key, S. Ji, W. Lv, R. Wang, Control of CuO nanocrystal morphology from ultrathin willow-leaf to flower-shaped for increased hydrazine oxidation activity, J. Power Sources 300 (2015) 344–350.
[10] M. Jafarian, T. Rostami, M.G. Mahjani, F. Gobal, A low cost and highly active non-noble alloy electrocatalyst for hydrazine oxidation based on nickel ternary alloy at the surface of graphite electrode, J. Electroanal. Chem. 763 (2016) 134–140.
[11] Z. Pu, C. Zhang, I.S. Amiinu, W. Li, L. Wu, S. Mu, General strategy for the synthesis of transition-metal phosphide/N-doped carbon frameworks for hydrogen and oxygen evolution, ACS Appl. Mater. Interfaces 9 (2017) 16187–16193.
[12] X. Huang, X. Zou, Y. Meng, E. Mikmeková, H. Chen, D. Voiry, A. Goswami, M. Chhowalla, T. Asefa, Yeast cells-derived hollow core/shell heteroatom-doped carbon microparticles for sustainable electrocatalysis, ACS Appl. Mater. Interfaces 7 (2015) 1978–1986.
[13] Y. Liang, Y. Zhou, J. Ma, J. Zhao, Y. Chen, Y. Tang, T. Lu, Preparation of highly dispersed and ultrafine Pd/C catalyst and its electrocatalytic performance for hydrazine electrooxidation, Appl. Catal. B Environ. 103 (2011) 388–396.
[14] M. Borghei, N. Laocharoen, E. Kibena-Põldsepp, L.S. Johansson, J. Campbell, E. Kauppinen, K. Tammeveski, O.J. Rojas, Porous N,P-doped carbon from coconut shells with high electrocatalytic activity for oxygen reduction: alternative to Pt-C for alkaline fuel cells, Appl. Catal. B Environ. 204 (2017) 394–402.
[15] Y. Meng, X. Zou, X. Huang, A. Goswami, Z. Liu, T. Asefa, Polypyrrole-derived nitrogen and oxygen Co-doped mesoporous carbons as efficient metal-free electrocatalyst for hydrazine oxidation, Adv. Mater. 26 (2014) 6510–6516.
[16] P. Serp, B. Machado, Carbon (Nano)materials for Catalysis, Nanostructured Materials for Catalysis, RSC Catalysis Series, Royal Society of Chemistry, Cambridge, UK, 2015, pp. 1–45 Chapter 1.
[17] D. Yu, E. Nagelli, F. Du, L. Dai, Metal-free carbon nanomaterials become more active than metal catalysts and last longer, J. Phys. Chem. Lett. 1 (2010) 2165–2173.
[18] A.C. Martins, X. Huang, A. Goswami, K. Koh, Y. Meng, V.C. Almeida, T. Asefa, Fibrous porous carbon electrocatalysts for hydrazine oxidation by using cellulose filter paper as precursor and self-template, Carbon 102 (2016) 97–105.
[19] S. Bag, B. Mondal, A.K. Das, C.R. Raj, Nitrogen and sulfur dual-doped reduced graphene oxide: synergistic effect of dopants towards oxygen reduction reaction, Electrochim. Acta 163 (2015) 16–23.
[20] A. Farzaneh, N. Saghatoleslami, E.K. Goharshadi, H. Gharibi, H. Ahmadzadeh, 3-D mesoporous nitrogen-doped reduced graphene oxide as an efficient metal-free electrocatalyst for oxygen reduction reaction in alkaline fuel cells: role of π and lone pair electrons, Electrochim. Acta 222 (2016) 608–618.
[21] D. Chen, J. Jiang, X. Du, Electrocatalytic oxidation of nitrite using metal-free nitrogen-doped reduced graphene oxide nanosheets for sensitive detection, Talanta 155 (2016) 329–335.
[22] R.I. Jafri, N. Rajalakshmi, K.S. Dhathathreyan, S. Ramaprabhu, Nitrogen doped graphene prepared by hydrothermal and thermal solid state methods as catalyst supports for fuel cell, Int. J. Hydrogen Energy 40 (2015) 4337–4348.
[23] D. Yu, L. Wei, W. Jiang, H. Wang, B. Sun, Q. Zhang, K. Goh, R. Si, Y. Chen, Nitrogen doped holey graphene as an efficient metal-free multifunctional electrochemical catalyst for hydrazine oxidation and oxygen reduction, Nanoscale 5 (2013) 3457–3464.
[24] G. Jiang, B. Peng, Waste cotton-derived N-doped carbon as a sustainable metal-free electrocatalyst for oxygen reduction, Mater. Lett. 188 (2017) 33–36.

[25] N. Liu, L. Ding, H. Li, M. Jia, W. Zhang, N. An, X. Yuan, N-doped nanoporous carbon as efficient catalyst for nitrobenzene reduction in sulfide-containing aqueous solutions, J. Colloid Interface Sci. 490 (2017) 677–684.
[26] A. Mulyadi, Z. Zhang, M. Dutzer, W. Liu, Y. Deng, Facile approach for synthesis of doped carbon electrocatalyst from cellulose nanofibrils toward high-performance metal-free oxygen reduction and hydrogen evolution, Nano Energy 32 (2017) 336–346.
[27] E. Granot, B. Filanovsky, I. Presman, I. Kuras, F. Patolsky, Hydrazine/air direct-liquid fuel cell based on nanostructured copper anodes, J. Power Sources 204 (2012) 116–121.
[28] A.L. Cazetta, S.P. Azevedo, O. Pezoti, L.S. Souza, A.M.M. Vargas, A.T. Paulino, J.C.G. Moraes, V.C. Almeida, Thermally activated carbon from bovine bone: optimization of synthesis conditions by response surface methodology, J. Anal. Appl. Pyrol. 110 (2014) 455–462.
[29] A.L. Cazetta, A.C. Martins, O. Pezoti, K.C. Bedin, K.K. Beltrame, T. Asefa, V.C. Almeida, Synthesis and application of N-S-doped mesoporous carbon obtained from nanocasting method using bone char as heteroatom precursor and template, Chem. Eng. J. 300 (2016) 54–63.
[30] J. Landers, G.Y. Gor, A.V. Neimark, Density functional theory methods for characterization of porous materials, Colloids Surf. A: Physicochem. Eng. Asp. 437 (2013) 3–32.
[31] W. Zhu, P. Robey, A. Boskey, Osteoporos 2 (2013) chapter 9, 150 p.
[32] Y. Sun, J. Wu, J. Tian, C. Jin, R. Yang, Sulfur-doped carbon spheres as efficient metal-free electrocatalysts for oxygen reduction reaction, Electrochim. Acta 178 (2015) 806–812.
[33] K.S.W. Sing, D.H. Everett, R.A.W. Haul, L. Moscou, R.A. Pierottu, J. Rouquérol, T. Siemieniewska, Reporting physisorption data for gas/solid systems with special reference to the determination of surface area and porosity, Pure Appl. Chem. 54 (1982) 603–619.
[34] M. Amjadi, J.L. Manzoori, T. Hallaj, N. Azizi, Sulfur and nitrogen co-doped carbon quantum dots as the chemiluminescence probe for detection of Cu2+ ions, J. Lumin. 182 (2017) 246–251.
[35] L. Yan, X. Bo, Y. Zhang, L. Guo, Facile green synthesis of nitrogen-doped porous carbon and its use for electrocatalysis towards nitrobenzene and hydrazine, Electrochim. Acta 137 (2014) 693–699.
[36] Y. Pang, H. Gao, S. Wu, X. Li, Facile synthesis the nitrogen and sulfur co-doped carbon dots for selective fluorescence detection of heavy metal ions, Mater. Lett. 193 (2017) 236–239.
[37] S. Ratso, I. Kruusenberg, U. Joost, R. Saar, K. Tammeveski, Enhanced oxygen reduction reaction activity of nanotube catalysts in alkaline media, Int. J. Hydrogen Energy 41 (2016) 22510–22519.
[38] Y.-B. Huang, Y. Fu, Hydrolysis of cellulose to glucose by solid acid catalysts, Green Chem. 15 (2013) 1095–1111.
[39] A. Martínez de Yuso, M. De Fina, C. Nita, P. Fioux, J. Parmentier, C. Matei Ghimbeu, Synthesis of sulfur-doped porous carbons by soft and hard templating processes for CO2 and H2 adsorption, Microporous Mesoporous Mater. 243 (2017) 135–146.
[40] L. Cao, Z. Lin, J. Huang, X. Yu, X. Wu, B. Zhang, Y. Zhan, F. Xie, W. Zhang, J. Chen, W. Xie, W. Mai, H. Meng, Nitrogen doped amorphous carbon as metal free electrocatalyst for oxygen reduction reaction, Int. J. Hydrogen Energy 42 (2017) 876–885.
[41] V. Perazzolo, E. Gradzka, C. Durante, R. Pilot, N. Vicentini, G.A. Rizzi, G. Granozzi, A. Gennaro, Chemical and electrochemical stability of nitrogen and sulphur doped mesoporous carbons, Electrochim. Acta 197 (2016) 251–262.
[42] X. Cui, Y. Wang, J. Liu, Q. Yang, B. Zhang, Y. Gao, Y. Wang, G. Lu, Dual functional N- and S-co-doped carbon dots as the sensor for temperature and Fe3+ ions, Sens. Actuators B: Chem. 242 (2017) 1272–1280.
[43] M. Klingele, C. Pham, K.R. Vuyyuru, B. Britton, S. Holdcroft, A. Fischer, S. Thiele, Sulfur doped reduced graphene oxide as metal-free catalyst for the oxygen reduction reaction in anion and proton exchange fuel cells, Electrochem. Commun. 77 (2017) 71–75.
[44] Y. She, Z. Lu, M. Ni, L. Li, M.K.H. Leung, Facile synthesis of nitrogen and sulfur codoped carbon from ionic liquid as metal-free catalyst for oxygen reduction reaction, ACS Appl. Mater. Interfaces 7 (2015) 7214–7221.
[45] J. Duan, S. Chen, M. Jaroniec, S.Z. Qiao, Heteroatom-doped graphene-based materials for energy-relevant electrocatalytic processes, ACS Catal. 5 (2015) 5207–5234.
[46] X.L. Wang, Y.X. Zheng, M.L. Jia, L.S. Yuan, C. Peng, W.H. Yang, Formation of nanoporous NiCuP amorphous alloy electrode by potentiostatic etching and its application for hydrazine oxidation, Int. J. Hydrogen Energy 41 (2016) 8449–8458.
[47] Y. Zhao, J. Zhao, Z. Su, D. Ma, X. Hao, Y. Lu, J. Guo, Room temperature synthesis of Cu nanocages through Ni-induced electroless process, Colloids Surf. A: Physicochem. Eng. Asp. 431 (2013) 60–65.
[48] X. Ma, J. Wang, D. Liu, R. Kong, S. Hao, G. Du, A.M. Asiri, X. Sun, Hydrazine-assisted electrolytic hydrogen production: CoS2 nanoarray as a superior bifunctional electrocatalyst, New J. Chem. 41 (2017) 4754–4757.
[49] C. Tang, R. Zhang, W. Lu, Z. Wang, D. Liu, S. Hao, G. Du, A.M. Asiri, X. Sun, Energy-saving electrolytic hydrogen generation: Ni2P nanoarray as a high-performance non-noble-metal electrocatalyst, Angew. Chem. Int. Ed. 56 (2017) 842–846.
[50] J. Wang, R. Kong, A.M. Asiri, X. Sun, Replacing oxygen evolution with hydrazine oxidation at the anode for energy-saving electrolytic hydrogen production, ChemElectroChem 4 (2017) 481–484.
[51] J. Wang, X. Ma, T. Liu, D. Liu, S. Hao, G. Du, R. Kong, A.M. Asiri, X. Sun, NiS2 nanosheet array: a high-active bifunctional electrocatalyst for hydrazine oxidation and water reduction toward energy-efficient hydrogen production, Mater. Today Energy 3 (2017) 9–14.
[52] L. Zhang, D. Liu, S. Hao, L. Xie, F. Qu, G. Du, A.M. Asiri, X. Sun, Electrochemical hydrazine oxidation catalyzed by iron phosphide nanosheets array toward energy-efficient electrolytic hydrogen production from water, ChemistrySelect 2 (2017) 3401–3407.
[53] V. Rao, Hariyanto, C. Cremers, U. Stimming, Investigation of the ethanol electro-oxidation in alkaline membrane electrode assembly by differential electrochemical mass spectrometry, Fuel Cells 7 (2007) 417–423.
[54] S.M. Golabi, M. Jalil, Electrocatalytic oxidation of hydrazine at Epinephrine modified glassy carbon electrode (EPMGCE), Iran. J. Chem. Chem. Eng. 22 (2003) 43–54.
[55] L. Yan, X. Bo, Y. Zhang, L. Guo, Facile green synthesis of nitrogen-doped porous carbon and its use for electrocatalysis towards nitrobenzene and hydrazine, Electrochim. Acta 137 (2014) 693–699.
[56] D. Yu, L. Wei, W. Jiang, H. Wang, B. Sun, Q. Zhang, K. Goh, R. Si, Y. Chen, Nitrogen doped holey graphene as an efficient metal-free multifunctional electrochemical catalyst for hydrazine oxidation and oxygen reduction, Nanoscale 5 (2013) 3457–3464.